BIOCHEMISTRY

 Volume 43, Number 41 October 19, 2004

Accelerated Publications

Preventing Misfolding of the Prion Protein by Trimethylamine *N*-Oxide[†]

Brian J. Bennion,[‡,§] Mari L. DeMarco,[‡,||] and Valerie Daggett*[,‡,||]

Department of Medicinal Chemistry and Biomolecular Structure and Design Program, University of Washington, Seattle, Washington 98195-7610

Received June 29, 2004; Revised Manuscript Received August 31, 2004

ABSTRACT: Transmissible spongiform encephalopathies are a class of fatal neurodegenerative diseases linked to the prion protein. The prion protein normally exists in a soluble, globular state (PrP^C) that appears to participate in copper metabolism in the central nervous system and/or signal transduction. Infection or disease occurs when an alternatively folded form of the prion protein (PrP^{Sc}) converts soluble and predominantly α-helical PrP^C into aggregates rich in β-structure. The structurally disordered N-terminus adopts β-structure upon conversion to PrP^{Sc} at low pH. Chemical chaperones, such as trimethylamine *N*-oxide (TMAO), can prevent formation of PrP^{Sc} in scrapie-infected mouse neuroblastoma cells [Tatzelt, J., *et al.* (1996) *EMBO J. 15*, 6363−6373]. To explore the mechanism of TMAO protection of PrP^C at the atomic level, molecular dynamics simulations were performed under conditions normally leading to conversion (low pH) with and without 1 M TMAO. In PrP^C simulations at low pH, the helix content drops and the N-terminus is brought into the small native β-sheet, yielding a PrP^{Sc}-like state. Addition of 1 M TMAO leads to a decreased radius of gyration, a greater number of protein−protein hydrogen bonds, and a greater number of tertiary contacts due to the N-terminus forming an Ω-loop and packing against the structured core of the protein, not due to an increase in the level of extended structure as with the PrP^C to PrP^{Sc} simulation. In simulations beginning with the "PrP^{Sc}-like" structure (derived from PrP^C simulated at low pH in pure water) in 1 M TMAO, similar structural reorganization at the N-terminus occurred, disrupting the extended sheet. The mechanism of protection by TMAO appears to be exclusionary in nature, consistent with previous theoretical and experimental studies. The TMAO-induced N-terminal conformational change prevents residues that are important in the conversion of PrP^C to PrP^{Sc} from assuming extended sheet structure at low pH.

Prion diseases affect the central nervous system and are a result of a conformational change in the prion protein (PrP),[1] often leading to prion protein-based plaques (*1*, *2*). In humans, these diseases can be sporadic, inherited, or infectious disorders (*3*, *4*). PrP is responsible for the following diseases in humans: Kuru, Gerstmann-Sträussler-Scheinker disease (GSS), fatal familial insomnia (FFI), Creutzfeldt-Jakob disease (CJD), and the BSE-linked, variant Creutzfeldt-Jakob disease (vCJD) (*5*−*7*). These diseases are always fatal. The infectious nature of this disease differs from that of other

[†] We gratefully acknowledge support from the National Institutes of Health (Grant RO1 GM-50789 to V.D.) and a National Institute of General Medical Sciences National Research Service Award (Grant GM-07750 to B.J.B. and M.L.D.).

* To whom correspondence should be addressed: Department of Medicinal Chemistry, University of Washington, Seattle, WA 98195-7610. E-mail: daggett@u.washington.edu. Fax: (206) 685-3252.

[‡] Department of Medicinal Chemistry.

[§] Current address: Lawrence Livermore National Laboratory, 7000 East Ave., Livermore, CA 94551.

[||] Biomolecular Structure and Design Program.

[1] Abbreviations: PrP, prion protein; PrP^C, cellular prion protein; PrP^{Sc}, scrapie prion protein; TMAO, trimethylamine *N*-oxide; MD, molecular dynamics.

10.1021/bi0486379 CCC: $27.50
Published on Web 09/25/2004

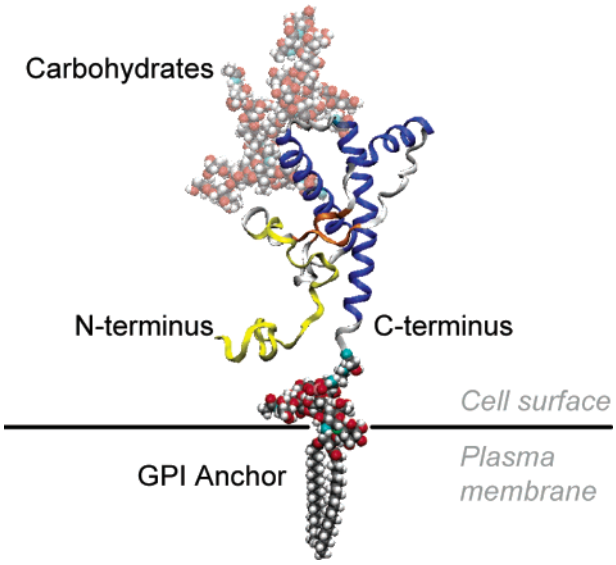

FIGURE 1: Model of the soluble hamster prion protein. Residues 125−228 are from the NMR structure (*20*) modeled with carbohydrates (space-filling representation, background), the unstructured N-terminal region (residues 90−124) (yellow), and the GPI-membrane anchor (space-filling representation, foreground). The structured domain of PrP contains three helices (blue), helix A (residues 144−156), helix B (residues 172−193), and helix C (residues 200−227), β-strands (orange), S1 (residues 129−131), and S2 (residues 161−163). For further information regarding PrP^C glycoforms, see ref *21*. This figure was produced using VMD (*56*).

infectious diseases in that the pathogen is a proteinaceous particle, lacking nucleic acids; thus, the "protein-only" hypothesis was proposed (*8*, *9*).

PrP^C is a monomeric, glycosylated, GPI-linked extracellular protein that appears to play a role in signal transduction (*10*) and/or in the maintenance of the proper copper ion concentration (*11*−*18*) (Figure 1). Other possible functions include a role in DNA metabolism and RNA binding (*19*). In contrast, the form linked to disease, the scrapie prion protein (PrP^{Sc} or PrP^{res}, for protease-resistant form), can adopt an oligomeric arrangement that has no known function, and it has yet to be structurally characterized by high-resolution methods. While the propagation of non-neuronal PrP^{Sc} is not necessarily pathogenic (*22*), the toxicity of neuronal PrP^{Sc} has been established (*23*). PrP^{Sc} is chemically indistinguishable from the normal, cellular prion protein (PrP^C or PrP^{sen}, for the protease-sensitive form) (*24*); however, their secondary and tertiary structures differ (*25*−*30*). Fourier transform infrared (FTIR) and circular dichroism (CD) spectroscopy studies indicate that PrP^C is highly helical (42%) with little β-sheet structure (3%) (*29*). In contrast, PrP^{Sc} contains a large amount of β-structure (43−54%) and less helical structure (17−30%) (*29*, *31*). The difference in secondary structure between PrP^C and PrP^{Sc} is a useful parameter for discriminating between PrP species in both experimental and theoretical studies.

To address the lack of detailed structural information regarding the conversion process of the prion protein, we have undertaken molecular dynamics (MD) simulations to model the conversion pathway of PrP^C. Beginning with a 111-residue fragment of PrP^C (residues 109−219, which contain the region known to convert; unfortunately, residues 90−108 are unstructured in PrP^C), we destabilize the protein by lowering the pH (*32*−*34*), which is how conversion is triggered *in vitro* (*35*) and how it is believed to occur *in vivo* (*30*). Such an approach can provide atomic-resolution information about the conversion process as well as possible PrP^{Sc} models. The term PrP^{Sc} is used to denote the scrapie, infectious form of the protein or more loosely the misfolded, β-rich conformer in the absence of information regarding infectivity. Here we use the term to denote a misfolded species of PrP^C that shares characteristics with PrP in aggregates (both soluble and insoluble; i.e., we do not know if our conformations are infectious). In a previous MD study (*32*), we observed the conversion of the NMR structure of Syrian hamster (SHa) PrP^C (Figure 2, A → B). ShaPrP under low-pH conditions adopts more β-like structure and loses helical structure, consistent with FTIR and CD spectroscopy experiments with PrP^{Sc} fibrils (*29*, *31*).

A previous study by Tatzelt and co-workers showed that trimethylamine *N*-oxide (TMAO) and other protective osmolytes prevent scrapie formation *in vitro* (*36*). TMAO, glycerol, and dimethyl sulfoxide (DMSO) were added to PrP^{Sc}-infected mouse neuroblastoma cells. These osmolytes reduced the extent of PrP^{Sc} formation, with TMAO being the most effective (75% reduction of PrP^{Sc} with 120 mM TMAO). However, deleterious effects on cellular function were noted for both DMSO and TMAO at higher concentrations. Glycerol was well tolerated but required higher concentrations (1 M) for the same effect. A later study of the effects of DMSO on scrapie-infected hamsters showed prolonged incubation times and a lower level of PrP^{Sc} accumulation *in vivo* (*37*). Nandi and co-workers (*38*) reported detectable structural destabilization of soluble mouse and sheep PrP^C in the presence of the "stabilizing" anion, SO_4^{2-}. Interactions of sulfate with the ~30 glycine residues at the N-terminus of the protein were posited to be the cause of the destabilization (*38*).

Our previous work looking at the effect of the stabilizing osmolyte TMAO on model peptides suggests that the effects of TMAO are mainly indirect at low concentrations (*39*). In the same study, we showed through both experiment and MD simulations that the driving force of TMAO-induced stability is the unfavorable enthalpic interactions of TMAO-influenced water with the peptide backbone. A later study of the effects of TMAO and urea on chymotrypsin inhibitor 2 supported the water-mediated stabilizing effect of TMAO (*40*). These results led us to examine the stabilizing effects of TMAO on other proteins, especially those relevant to protein unfolding and/or misfolding diseases.

In this work, we employ MD to determine the effects of TMAO on the dynamics and structure of the prion protein at the atomic level. We show that the misfolded, PrP^{Sc}-like prion protein obtained via MD simulation under acidic conditions (which we call PrP^{Sc}) can be restored to a more globular structure upon addition of 1 M TMAO. Furthermore, in MD simulations of PrP^C under acidic conditions with 1 M TMAO, the N-terminal portion of the protein minimizes its level of solvent exposure by making additional contacts with the main body of the protein and conversion to PrP^{Sc} is prevented.

METHODS

MD simulations were performed using ENCAD (*41*) and associated protocols published elsewhere (*42*−*44*). In total,

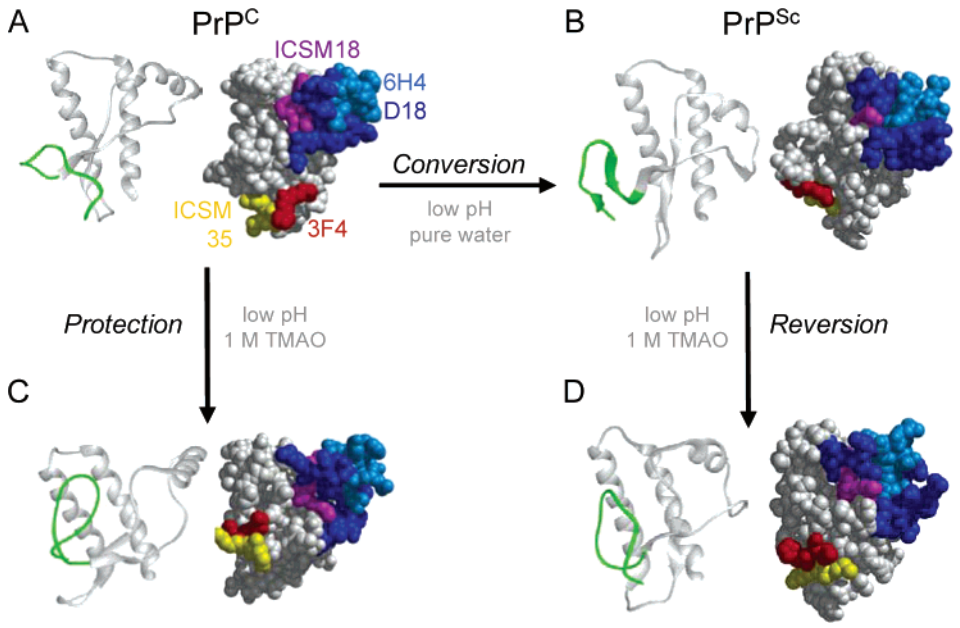

FIGURE 2: Snapshots from molecular dynamics simulations of the hamster prion protein in ribbon and space-filling representations: A → B, conversion simulation of the prion protein; A → C, protection simulation of the prion protein; and B → D, reversion simulation of the prion protein. (A) Minimized Syrian hamster NMR structure of PrP^C. (B) PrP after MD simulation for 10 ns at low pH yielding a PrP^{Sc}-like structure rich in extended structure. (C) Snapshot of the 10 ns structure from MD simulation (first protection simulation) at low pH in 1 M TMAO, which used the NMR structure (A) as the initial coordinates. (D) Snapshot of the 10 ns structure from MD simulation (first reversion trajectory) at low pH in 1 M TMAO using panel B as the starting structure. Common epitopes used to experimentally characterize PrP are shown in the space-filling model and include antibody binding sites for ICSM 35 (yellow), 3F4 (red), ICSM 18 (magenta), 6H4 (cyan), and D18 (blue). The dynamic N-terminus (residues 109−128) is colored green in the ribbon diagrams. Protein structure images were produced using MIDASPLUS (University of California, San Franscisco, CA) (*55*).

one PrP^C (native state), one $PrP^C \rightarrow PrP^{Sc}$ (conversion simulation), two PrP^C + TMAO (protection simulations), and two PrP^{Sc} + TMAO (reversion simulations) simulations were run at 25 °C for 10 ns each. The native state (neutral pH) and the $PrP^C \rightarrow PrP^{Sc}$ (low pH) simulations of the hamster prion protein were described previously (*32*). The 10 ns structure from the $PrP^C \rightarrow PrP^{Sc}$ simulation was used as the starting point for the reversion (PrP^{Sc} + TMAO) simulation. Residues 109−219 of NMR structure 4 of the hamster prion protein [PDB entry 1B10 (*20*)] were used as the starting point for the protection (PrP^C + TMAO) simulation. Both the protection and reversion simulations were conducted at low pH by protonating all histidine, aspartate, and glutamate amino acids. First, a box of water was constructed giving a distance of at least 8 Å around the protein. TMAO was then added to the system by randomly swapping waters for TMAO until the mole fraction (0.02) equivalent to a 1 M TMAO solution was reached (*44*). The swapping resulted in 81 molecules of TMAO and 3969 water molecules being in the protection simulations. The reversal simulations contained 91 TMAO molecules and 4471 water molecules. The density of the system was set to the experimental density, 0.9996 g/mL (M. Auton and W. Bolen, personal communication), by adjusting the volume of the simulation box. The microcanonical ensemble (NVE) was used in our MD simulations so that the volume remained constant throughout each trajectory. Periodic boundary conditions and the minimum image convention were employed in the energy calculations. The nonbonded interaction list was updated every fifth step of dynamics, and structures were saved every 0.2 ps for analysis. Duplicate trajectories were calculated by altering water and TMAO positions within the simulation boxes. Within 3 ns, the first protection and both reversion simulations converged; after this point, there was little change in the protein's properties over time.

RESULTS

Several independent simulations were performed to investigate the influence of TMAO on the prion protein: PrP^C at low pH in water, yielding PrP^{Sc}-like structures (conversion); PrP^C + 1 M TMAO (protection); and PrP^{Sc} + 1 M TMAO (reversion).

A qualitative assessment of conformational change and its biological relevance was achieved by monitoring known antibody binding epitopes for accessibility and/or continuity over the course of each simulation. To assess quantitatively the changes to the overall structure of the protein, several general characteristics were measured: solvent accessibility (SASA), radius of gyration, secondary structure, intraprotein contacts, and protein−protein hydrogen bonds.

Since TMAO has been shown to exert its effect on model peptides and proteins indirectly through its interactions with water at this concentration (*40*, *44*), water self-diffusion and hydrogen bonding properties of the solvent were also monitored.

Conversion. As seen previously (*32*), the $PrP^C \rightarrow PrP^{Sc}$ simulation at low pH showed significant motion at the N-terminus as β-strand-like secondary structure formed (Figure 2, A → B). In PrP^C, five segments of stable secondary structure are present: three α-helices and two β-strands (S1 and S2). During the conversion process, S1 and S2 nucleated the growth of new extended structure and HA partially unfolded to accommodate the new conformation. We term this new conformation PrP^{Sc} to denote that the protein has misfolded over the course of the simulation and that the

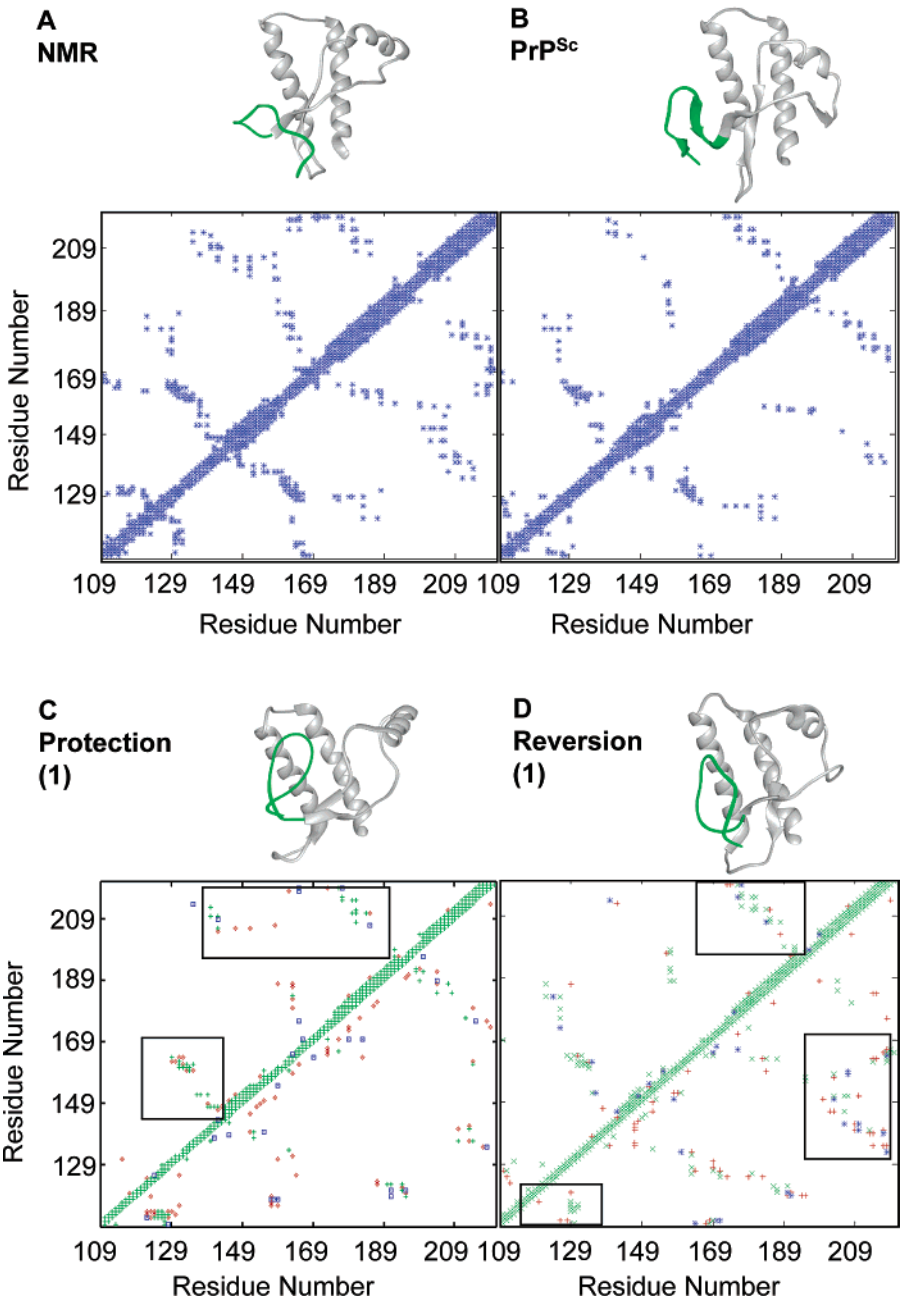

FIGURE 3: Tertiary contacts for the (A) NMR structure (*20*), (B) final structure from a previous $PrP^C \rightarrow PrP^{Sc}$ conversion simulation in pure water (*32*), (C) native and non-native contacts in the first protection (PrP^C + TMAO) simulation, and (D) first reversion (PrP^{Sc} + TMAO) simulation. In panels C and D, contacts that persisted for greater than 80% of the analysis time are colored blue, contacts formed between 60 and 80% of the analysis time are colored green, and contacts lasting less than 60% of the analysis time are colored red. For panels C and D, contacts remaining from the NMR structure (C) and conversion simulation (D) are plotted in the top left half of each plot. New contacts formed during the simulations are plotted in the bottom right half of each plot. Tertiary contacts were counted when heavy atom distances were <5.4 Å for carbon−carbon contacts and <4.6Å between carbon and polar heavy atoms for residues that were at least one residue apart in sequence. Only the first interaction was counted as a contact, whereas additional contacts between the same residues at the same time point were ignored. The 10 ns structure is shown above its respective panel in ribbon format. Protein structure images were produced using MIDASPLUS (*55*).

misfolded species shares some of the physical characteristics of PrP found in aggregates (i.e., increased extended structure content and decreased α-helical content).

The conversion trajectory showed a decrease in SASA (as the sheet structure formed); the level of side chain exposure decreased by ∼400 Å^2, while the level of main chain exposure increased by ∼100 Å^2. The N-terminus was very dynamic and began extending out into the solution. As this extension proceeded, the protein became less globular.

The level of tertiary contacts decreased slightly in the simulation (Figure 3). Further examination of the contacts on a per residue basis showed that many native contacts were lost during conversion as compared with the original NMR structure (Figure 3A,B). As the N-terminus moved, new non-native contacts were formed between residues 125 and 129 and between residues 109 and 111 (Figure 3B). A second set of non-native contacts also formed at the C-terminus between residues 195 and 208 (Figure 3B).

Table 1: Average Structural Properties of the Prion Protein at Low pH in 1 M TMAO[a]

		solvent accessible surface area (Å²)[b]		main chain solvent accessible surface area (Å²)[b]		radius of gyration (Å)[c]		tertiary contacts[d]		protein−protein hydrogen bonds	
		initial[e]	final[f]	initial[e]	final[f]	initial[e]	final[f]	initial[e]	final[f]	initial[e]	final[f]
$PrP^C \rightarrow PrP^{Sc}$	conversion	8457 (270)	8065 (214)	1098 (45)	1179 (46)	14.8 (0.2)	14.5 (0.1)	353 (5)	344 (8)	66 (4)	61 (4)
PrP^C + TMAO	protection 1	9095 (219)	9136 (120)	1238 (48)	1220 (27)	15.5 (0.2)	14.8 (0.1)	315 (7)	318 (6)	55 (5)	60 (3)
	protection 2	8735 (141)	8727 (149)	1192 (69)	1246 (26)	15.0 (0.1)	15.2 (0.1)	328 (7)	333 (7)	63 (4)	64 (4)
PrP^{Sc} + TMAO	reversion 1	9568 (103)	8018 (126)	1339 (28)	1175 (25)	14.9 (0.1)	13.9 (0.1)	310 (5)	342 (7)	54 (4)	63 (4)
	reversion 2	9665 (184)	8139 (112)	1399 (43)	1123 (24)	14.9 (0.1)	14.1 (0.1)	301 (8)	354 (8)	52 (5)	66 (4)

[a] For each property, the average value was determined from either the initial 100 ps or the final 2 ns of each trajectory. Standard deviations of average values are given in parentheses. [b] The total solvent accessible surface area was calculated using an in-house version of NACCESS (*57*). [c] The radius of gyration was calculated by dividing the sum of the squared, pairwise distances between Cα atoms by the total number of Cα atoms. [d] See the text for a definition of a tertiary contact. [e] Average over the first 100 ps. Differences in initial values were a result of differences in system preparation. [f] Average over the last 2 ns of the simulation (8−10 ns).

Protection. Simulations of PrP^C in 1 M TMAO demonstrated some interesting structural features. In the first of these protection simulations, the N-terminus packed against the protein in an Ω-loop (Figure 2C). Ω-Loops are regions of nonregular secondary structure formed by a sequence that follows an Ω-shaped path (*45*). In the first protection simulation, an Ω-loop formed in the sequence from residue 111 to 124. The opposing "strands" in the loop were closely packed with nonrepeating (Φ and Ψ) angles characteristic of an Ω-loop. While no Ω-loop formed during the course of the second protection simulation, the dynamic behavior of the N-terminus was similar to the early events in the first simulation. This suggested that the second simulation was following a similar pathway. In both simulations, the native secondary structure of the structured region of PrP^C was stabilized. In a 1 M TMAO solution at low pH, helix A remained helical and rigidly packed against helix C, contrasting with the conversion simulation (pure water) in which low pH destabilized helix A.

To compare simulation to experiment, we inspected the accessibility of various PrP antibody binding epitopes. In Figure 2, common epitopes are colored and displayed on the surface of the protein for PrP^C (the NMR structure), PrP^{Sc}, and final structures from the TMAO trajectories. All epitopes were still accessible to the solvent (Figure 2) after simulation for 10 ns. While the N-terminal PrP^C-selective 3F4 epitope remained accessible, it was in a conformation different from that in the NMR structure (Figure 2).

The two protection simulations showed little deviation in total SASA throughout the simulation. Changes in the radius of gyration in the presence of TMAO were modest and correlated with the dynamics of the N-terminus (Table 1). Contact analysis data were in agreement with the very slight changes in conformation of PrP in both simulations as a majority of native contacts were preserved. In the first simulation, a small number of contacts were lost (i.e., residue 129 to residues 110−118), a few shifted by one or two residues (residues 135−140 to residues 209−215), and nonnative contacts (residues 120−132 to residues 112−115) appeared as a result of the Ω-loop (Figure 3C).

The helical content increased approximately 10% in the presence of 1 M TMAO, while the β-content dropped 10−15%. All three of the native helices became stronger (based on propensities of residues to be in helical conformations over the course of the simulation) and longer. Several residues in the N-terminus, particularly residues 118−124, also showed stronger helical tendencies, while no regular helical structure formed in that region. The overall β-structure content decreased due to the loss of S1 and large fluctuations in S2, which oscillated between 20 and 80% β-structure. The S1−S2 sheet remained native-like, but the β-structure content decreased as the Φ and Ψ angles of the native β-sheet residues drifted outside of our strict β-conformation range.

Reversion. Strikingly, both simulations starting with PrP^{Sc} in 1 M TMAO resulted in reversion from a misfolded species to one with more native-like structural characteristics. In the two trajectories, the non-native extended structure of PrP^{Sc} dissolved to form an Ω-loop at the N-terminus (Figure 2). The Ω-loop formed over residues 110−122 in the first simulation and over residues 111−128 in the second (the latter loop being less compact). Both loops formed at the surface of the protein and maintained interactions with helix B. These N-terminal motions and other changes in the proteins in the presence of TMAO caused the protein to become more globular.

In the first reversion simulation, the trajectory began with the 3F4 epitope being partially obstructed by the extended sheet at the N-terminus (Figure 2B). Over the course of the simulation, the extended sheet dissolved and the 3F4 epitope re-formed at the protein surface (Figure 2D).

Both reversion simulations showed a significant decrease in SASA (Table 1). The decrease in SASA for the reversal simulations was mostly due to burial of nonpolar side chains: from 5483 to 4427 Å² (reversion 1) and from 5563 to 4530 Å² (reversion 2). A significant decrease in the main chain SASA occurred in both reversion simulations for an average drop from 1369 to 1149 Å², in contrast to the simulation of PrP in pure water at low pH. Reversion trajectories displayed the greatest decrease in radius of gyration (Table 1), correlated with the burial of nonpolar residues, Ω-loop formation, and improved packing (Table 1 and Figure 2).

Many native contacts that were lost in the conversion simulation were restored in the reversion simulations. For example, native contacts between residues 199−219 and 128−168 were re-formed in the reversion simulations (Figure 3D). Other native contacts were gained and/or strengthened at the N-terminus (residues 127−129 to 109−119) in the presence of 1 M TMAO (Figure 3D). Some residual nonnative PrP^{Sc} contacts persisted in the presence of TMAO (for example, residues 123−128 to residue 110 and residues 183−189 to residues 200−209). Overall, the reversion structures regained native helical structure in helix A, restored native packing of helix A to the hydrophobic core, and

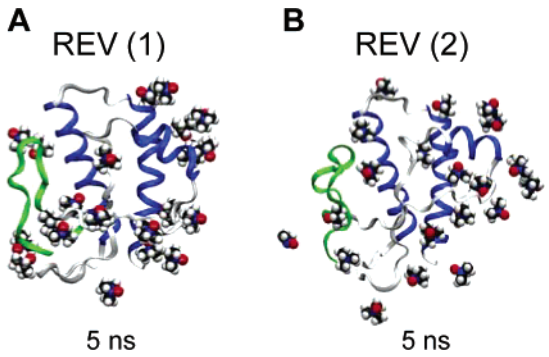

FIGURE 4: TMAO molecules (space-filling) surrounding PrP (ribbon). Images are from the 5 ns structures from the first (A) and second (B) reversion trajectories and show only TMAO molecules within 3.5 Å of any protein atom. N-Terminal residues 109−128 are colored green, and helices are colored blue. This figure was produced using VMD (*56*).

converted the non-native extended structure in the N-terminus to an Ω-loop.

The behavior of the β-structure in the reversion simulations was similar to the protection simulations described above; S1 dissolved, and S2 fluctuated between 30 and 90% β-structure. The overall helicity remained at ∼50%, while the average β-strand content decreased 5%. Helix A regained some but not all of its native helix from its unwound starting point in PrP^{Sc}. The helicity in helices B and C remained constant throughout. There were also residues in the N-terminus that adopted helical character, although no well-structured non-native helices formed.

Solvent Properties. Water dynamics and structure were analyzed for simulations with and without TMAO to explore the effects of TMAO on the solvent environment. The water self-diffusion coefficient was calculated by the Einstein method (*44*) and was slower in the simulations with 1 M TMAO present (0.16−0.17 $Å^2$/ps) when compared to values for simulations in pure water, i.e., the conversion simulation (0.22 $Å^2$/ps). These data are in agreement with previous simulations (*40*, *44*) and experiment (*46*). Our previous work has shown that the distribution of water−water distances is affected by the presence of a cosolvent (*40*, *44*). The average number of hydrogen bonds per water molecule was measured in the hydration layer and was 3.06 in both the conversion simulation and TMAO (protection and reversion) simulations. The number of hydrogen bonds per water in the bulk was similar (3.30).

Approximately 10% of the TMAO molecules interacted directly with the protein (Figure 4) in hydrogen bonds with Arg, Lys, and His residues. The average TMAO−side chain bond length was ∼1.6 Å. These hydrogen bonds were fairly long-lived (∼1 ns), although exchange did occur during the course of the simulations. Hydrogen bonds with the peptide backbone were sporadic and minimal, involving only three to four TMAO molecules during the 10 ns simulations. Nonpolar contacts between TMAO methyl groups and hydrophobic surface residues were also observed and involved an additional 10% of the total TMAO present. The number of waters in the hydration layer was similar in both the conversion and TMAO simulations (∼260 waters). We also monitored the distribution of water−water hydrogen bond lengths for the water in the hydration shell and in bulk. The number of very strong bulk water−water bonds (N−H···O═C distance = 1.2−1.6 Å) in the 1 M TMAO solutions was 32% greater than in the pure water solution. The same trend was observed in the hydration shell: 666 strong hydrogen bonds in pure water compared with 770 such hydrogen bonds in the presence of 1 M TMAO.

DISCUSSION

Work by Tatzelt and co-workers (*36*) showing a reduced level of $PrP^C \rightarrow PrP^{Sc}$ conversion in the presence of osmolytes is intriguing and warrants study at the atomic level. Our previous studies with TMAO and urea suggest that relatively low concentrations of TMAO affect protein structure and dynamics (*40*). Furthermore, we have been able to simulate the $PrP^C \rightarrow PrP^{Sc}$ conversion triggered by low pH (*32*−*34*). Here we build on these previous studies to explore the effect of TMAO on the conformational behavior of the prion protein.

In general, the solvent accessible surface area of PrP either remained constant or decreased in the presence of 1 M TMAO (Table 1). The helical content in the presence of TMAO increased as a result of the strengthening of the native helices. No new helices formed, which is consistent with the previously reported behavior of TMAO not inducing non-native helical structure (*47*). In simulations beginning with a PrP^{Sc}-like conformation, TMAO led to increases in the number of native intraprotein contacts and hydrogen bonds (Table 1), suggesting that TMAO can rescue misfolded species by inducing PrP^C-like structural characteristics. This observation is consistent with experimental reports of the effect of TMAO on other systems, such as its ability to restore the enzymatic activity of enzymes in the presence of urea (*48*, *49*). The consistent loss of S1 and erratic fluctuations of S2 in the presence of TMAO were not expected and suggest that these elements of secondary structure are sensitive to conformational change in the N-terminus and solvent environment. Since S1 can act as a template from which new extended strands can "grow" in conversion simulations (*32*−*34*), the disruption of S1 could be creating a barrier to PrP^{Sc} formation.

In our previous $PrP^C \rightarrow PrP^{Sc}$ simulations, the N-terminal portions of the 3F4 epitope disappeared as the N-terminus adopted β-structure (Figure 2), in agreement with the lack of binding of the 3F4 antibody to PrP^{Sc} *in vitro* (*50*). However, in the protection simulations, TMAO preserved the 3F4 epitope under conditions (low pH) that normally disrupt or bury the epitope. Furthermore, Tatzelt and co-workers (*34*) reported that D13, an antibody binding to residues 94−105 (*51*), did not bind to the prion protein in the presence of TMAO. Although our simulations did not include the N-terminal residues that comprise the D13 epitope, large conformational changes at the N-terminus in our TMAO simulations suggest these changes are responsible for the "disappearance" of the D13 binding site. It would be interesting to monitor antibody binding in the presence of TMAO for other antibodies. These experiments could provide more information about the conformation of the prion protein in TMAO.

Studies have suggested that the exclusion of the peptide backbone from the TMAO-affected solvent accounts for its stabilizing effect (*44*, *52*, *53*). In our previously published $PrP^C \rightarrow PrP^{Sc}$ simulations (*32*−*34*), the N-terminus exposed

a large number of amide groups to the solvent, which began to populate β-strand-like conformations. However, in the presence of 1 M TMAO, the N-terminus was excluded from the solvent, and made more contacts with the structured core of the protein to reduce the nonpolar surface area. These observations are consistent with the peptide exclusion hypothesis. Given that there is an observable decrease in the main chain SASA and that our construct contains only 15 residues (109−124) of the possible 34-residue unstructured N-terminus (residues 90−124) usually included in experimental constructs, researchers may observe a more dramatic change in SASA.

TMAO's effects on the solvent environment are significant, as indicated in the current work and in previous studies. The extent of water self-diffusion in the protection and reversal simulations decreased by ∼30% in the presence of TMAO, in good agreement with our previous work (*44*) and experiment (*47*). The reduction in the level of water diffusion inhibited the exchange of water from the surface of the protein and bulk. Earlier, we showed that the "sphere of influence" for each TMAO molecule extends out ∼6 Å (*44*). Water in the shell of TMAO was highly ordered but optimized interactions with itself so that it is has a slightly higher number of hydrogen bonds per water molecule than pure water (*44*). Introduction of diglycine cyclic peptides decreased the number of hydrogen bonds per water in the hydration layer and in bulk. The opposite occurred when cyclic dialanine was solvated in 1 M TMAO. Water thus altered may not fully interact with the protein and the peptide backbone due to the energetic penalty associated with breaking out of the TMAO sphere of influence (*44*) (Figure 4). On the other hand, water at the surface of the protein (not in the TMAO hydration shell) will be under the influence of the dynamics of the protein and not bulk water because of the penalty for exchange. The protein can then undergo conformational changes that optimize peptide−peptide interactions while minimizing peptide−water interactions.

The presence of 1 M TMAO in MD simulations of PrP caused the protein to favor PrP^C-like conformations. The native helical structure content was preserved or increased in the presence of TMAO at low pH. This finding is significant considering that low-pH conditions can cause helix A to unfold in pure water (Figure 2B). TMAO therefore is able to counteract the effects of low pH that disrupt helicity in PrP. The extended sheet structure content decreased in TMAO independent of starting structure. The radius of gyration, solvent accessible surface area, tertiary contacts, and intraprotein hydrogen bonds all indicated a more globular protein structure in the presence of TMAO under low-pH conditions. Water structure was also enhanced in the presence of TMAO. The organic solvent TMAO alters the solvation shell around the protein, weakening the competition between water−protein and protein−protein hydrogen bonds. Inhibiting water−protein hydrogen bonds increases the number of intraprotein hydrogen bonds, resulting in a more stable protein structure. The PrP^C-like structures derived from PrP^{Sc} by the addition of TMAO have a restored hydrophobic core. Similarly, in the protection simulations, the native core is preserved despite the low-pH environment. TMAO shifts the equilibrium away from the misfolded state and toward the native state.

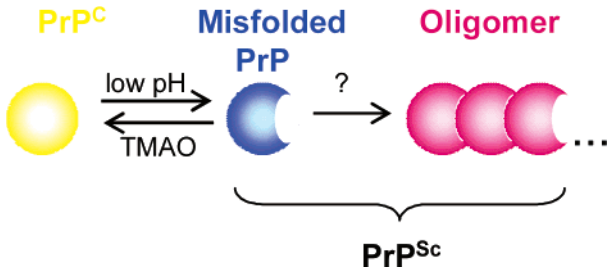

FIGURE 5: Schematic representation of the prevention and rescue of misfolded PrP, or PrP^{Sc}-like conformations, by TMAO.

Our simulations beginning with either PrP^C or PrP^{Sc} converge on similar structures in the presence of 1 M TMAO, a native-like PrP core with an Ω-loop in the region of the unstructured N-terminus, and experimentally, TMAO has been shown to inhibit PrP^{Sc} formation, suggesting that this structure is conversion resistant. The formation of an Ω-loop at the hydrophobic N-terminus allows partial burial of a potentially aggregate prone region. The Ω-loop may also stabilize the structured region of PrP^C by interacting with helix B. It has been proposed that in cases where Ω-loops make many hydrogen bonds or, as in our case, many hydrophobic interactions, they confer stability on the protein (*54*). Our results provide evidence that TMAO not only inhibits PrP^{Sc} formation but also can rescue early misfolded species along the conversion pathway (Figure 5).

ACKNOWLEDGMENT

We thank Drs. Patricia Campbell and Allan Rettie for their reading of the manuscript and insightful comments.

REFERENCES

1. DeArmond, S. J., McKinley, M. P., Barry, R. A., Braunfeld, M. B., McColloch, J. R., and Prusiner, S. B. (1985) Identification of prion amyloid filaments in scrapie-infected brain, *Cell 41*, 221−235.
2. Caughey, B. (2001) Interactions between prion protein isoforms: the kiss of death? *Trends Biochem. Sci. 26*, 235−242.
3. Prusiner, S. B. (1998) The prion diseases, *Brain Pathol. 8*, 499−513.
4. Cohen, F. E., and Prusiner, S. B. (1998) Pathologic conformations of prion proteins, *Annu. Rev. Biochem. 67*, 793−819.
5. Will, R. G., Ironside, J. W., Zeidler, M., Cousens, S. N., Estibeiro, K., Alperovitch, A., Poser, S., Pocchiari, M., Hofman, A., and Smith, P. G. (1996) A new variant of Creutzfeldt-Jakob disease in the U.K., *Lancet 347*, 921−925.
6. Horwich, A. L., and Weissman, J. S. (1997) Deadly conformations: protein misfolding in prion disease, *Cell 89*, 499−510.
7. Prusiner, S. B. (1997) Prion diseases and the BSE crisis, *Science 278*, 245−251.
8. Prusiner, S. B. (1998) Prions, *Proc. Natl. Acad. Sci. U.S.A. 95*, 13363−13383.
9. Griffith, J. S. (1967) Self-replication and scrapie, *Nature 215*, 1043−1044.
10. Mouillet-Richard, S., Ermonval, M., Chebassier, C., Laplanche, J. L., Lehmann, S., Launay, J. M., and Kellermann, O. (2000) Signal transduction through prion protein, *Science 289*, 1925−1928.
11. Burns, C. S., Aronoff-Spencer, E., Dunham, C. M., Lario, P., Avdievich, N. I., Antholine, W. E., Olmstead, M. M., Vrielink, A., Gerfen, G. J., Peisach, J., Scott, W. G., and Millhauser, G. L. (2002) Molecular features of the copper binding sites in the octarepeat domain of the prion protein, *Biochemistry 41*, 3991−4001.
12. Brown, D. R., Schmidt, B., and Kretzschmar, H. A. (1998) A prion protein fragment primes type 1 astrocytes to proliferation signals from microglia, *J. Neurochem. 70*, 1686−1693.

13. Qin, K., Yang, Y., Mastrangelo, P., and Westaway, D. (2002) Mapping Cu(II) binding sites in prion proteins by diethyl pyrocarbonate modification and matrix-assisted laser desorption ionization-time of flight (MALDI-TOF) mass spectrometric footprinting, *J. Biol. Chem. 277*, 1981−1990.
14. Qin, K., Coomaraswamy, J., Mastrangelo, P., Yang, Y., Lugowski, S., Petromilli, C., Prusiner, S. B., Fraser, P. E., Goldberg, J. M., Chakrabartty, A., and Westaway, D. (2003) The PrP-like protein Doppel binds copper, *J. Biol. Chem. 278*, 8888−8896.
15. Pushie, M. J., and Rauk, A. (2003) Computational studies of Cu(II)[peptide] binding motifs: Cu[HGGG] and Cu[HG] as models for Cu(II) binding to the prion protein octarepeat region, *J. Biol. Inorg. Chem. 8*, 53−65.
16. Garnett, A. P., and Viles, J. H. (2003) Copper binding to the octarepeats of the prion protein. Affinity, specificity, folding, and cooperativity: insights from circular dichroism, *J. Biol. Chem. 278*, 6795−6802.
17. Rachidi, W., Mange, A., Senator, A., Guiraud, P., Riondel, J., Benboubetra, M., Favier, A., and Lehmann, S. (2003) Prion infection impairs copper binding of cultured cells, *J. Biol. Chem. 278*, 14595−14598.
18. Rachidi, W., Vilette, D., Guiraud, P., Arlotto, M., Riondel, J., Laude, H., Lehmann, S., and Favier, A. (2003) Expression of prion protein increases cellular copper binding and antioxidant enzyme activities but not copper delivery, *J. Biol. Chem. 278*, 9064−9072.
19. Derrington, E., Gabus, C., Leblanc, P., Chnaidermann, J., Grave, L., Dormont, D., Swietnicki, W., Morillas, M., Marck, D., Nandi, P., and Darlix, J. L. (2002) PrPC has nucleic acid chaperoning properties similar to the nucleocapsid protein of HIV-1, *C. R. Acad. Sci. III 325*, 17−23.
20. James, T. L., Liu, H., Ulyanov, N. B., Farr-Jones, S., Zhang, H., Donne, D. G., Kaneko, K., Groth, D., Mehlhorn, I., Prusiner, S. B., and Cohen, F. E. (1997) Solution structure of Syrian hamster prion protein rPrP(90−231), *Proc. Natl. Acad. Sci. U.S.A. 94*, 10086−10091.
21. DeArmond, S. J., Qiu, Y., Sanchez, H., Spilman, P. R., Ninchak-Casey, A., Alonso, D., and Daggett, V. (1999) PrPc glycoform heterogeneity as a function of brain region: implications for selective targeting of neurons by prion strains, *J. Neuropathol. Exp. Neurol. 58*, 1000−1009.
22. Mallucci, G., Dickinson, A., Linehan, J., Klohn, P. C., Brandner, S., and Collinge, J. (2003) Depleting neuronal PrP in prion infection prevents disease and reverses spongiosis, *Science 302*, 871−874.
23. Legname, G., Baskakov, I. V., Nguyen, H. O., Riesner, D., Cohen, F. E., DeArmond, S. J., and Prusiner, S. B. (2004) Synthetic mammalian prions, *Science 305*, 673−676.
24. Stahl, N., Baldwin, M. A., Teplow, D. B., Hood, L., Gibson, B. W., Burlingame, A. L., and Prusiner, S. B. (1993) Structural studies of the scrapie prion protein using mass spectrometry and amino acid sequencing, *Biochemistry 32*, 1991−2002.
25. Basler, K., Oesch, B., Scott, M., Westaway, D., Walchli, M., Groth, D. F., McKinley, M. P., Prusiner, S. B., and Weissmann, C. (1986) Scrapie and cellular PrP isoforms are encoded by the same chromosomal gene, *Cell 46*, 417−428.
26. Caughey, B., Raymond, G. J., Ernst, D., and Race, R. E. (1991) *J. Virol. 65*, 6597−6603.
27. Stahl, N., and Prusiner, S. B. (1991) *FASEB J. 5*, 2799−2807.
28. Caughey, B., and Raymond, G. J. (1991) The scrapie-associated form of PrP is made from a cell surface precursor that is both protease- and phospholipase-sensitive, *J. Biol. Chem. 266*, 18217−18223.
29. Pan, K. M., Baldwin, M., Nguyen, J., Gasset, M., Serban, A., Groth, D., Mehlhorn, I., Huang, Z., Fletterick, R. J., Cohen, F. E., *et al*. (1993) Conversion of α-helices into *β*-sheets features in the formation of the scrapie prion proteins, *Proc. Natl. Acad. Sci. U.S.A. 90*, 10962−10966.
30. Kocisko, D. A., Priola, S. A., Raymond, G. J., Chesebro, B., Lansbury, P. T., Jr., and Caughey, B. (1995) Species specificity in the cell-free conversion of prion protein to protease-resistant forms: a model for the scrapie species barrier, *Proc. Natl. Acad. Sci. U.S.A. 92*, 3923−3927.
31. Caughey, B. W., Dong, A., Bhat, K. S., Ernst, D., Hayes, S. F., and Caughey, W. S. (1991) Secondary structure analysis of the scrapie-associated protein PrP 27−30 in water by infrared spectroscopy, *Biochemistry 30*, 7672−7680.
32. Alonso, D. O. V., DeArmond, S. J., Cohen, F. E., and Daggett, V. (2001) Mapping the early steps in the pH-induced conformational conversion of the prion protein, *Proc. Natl. Acad. Sci. U.S.A. 98*, 2985−2989.
33. Alonso, D. O. V., An, C., and Daggett, V. (2002) Simulations of biomolecules: Characterization of the early steps in the pH-induced conformational conversion of the hamster, bovine and human forms of the prion protein, *Philos. Trans. R. Soc. London, Ser. A 360*, 1−13.
34. DeMarco, M. L., and Daggett, V. (2004) From conversion to aggregation: protofibril formation of the prion protein, *Proc. Natl. Acad. Sci. U.S.A. 101*, 2293−2298.
35. Swietnicki, W., Petersen, R., Gambetti, P., and Surewicz, W. K. (1997) pH-dependent stability and conformation of the recombinant human prion protein PrP(90−231), *J. Biol. Chem. 272*, 27517−27520.
36. Tatzelt, J., Prusiner, S. B., and Welch, W. J. (1996) Chemical chaperones interfere with the formation of scrapie prion protein, *EMBO J. 15*, 6363−6373.
37. Shaked, G. M., Engelstein, R., Avraham, I., Kahana, E., and Gabizon, R. (2003) Dimethyl sulfoxide delays PrP^{Sc} accumulation and disease symptoms in prion-infected hamsters, *Brain Res. 983*, 137−143.
38. Nandi, P. K., Leclerc, E., and Marc, D. (2002) Unusual property of prion protein unfolding in neutral salt solution, *Biochemistry 41*, 11017−11024.
39. Zou, W. Q., and Cashman, N. R. (2002) Acidic pH and detergents enhance in vitro conversion of human brain PrP^{C} to a PrP^{Sc}-like form, *J. Biol. Chem. 277*, 43942−43947.
40. Bennion, B. J., and Daggett, V. (2004) Counteraction of urea-induced protein denaturation by trimethylamine *N*-oxide: a chemical chaperone at atomic resolution, *Proc. Natl. Acad. Sci. U.S.A. 101*, 6433−6438.
41. Levitt, M. (1990) *ENCAD: Energy Calculations and Dynamics*, Yeda, Rehovat, Israel.
42. Levitt, M., Hirshberg, M., Sharon, R., and Daggett, V. (1995) Potential energy function and parameters for simulations of the molecular dynamics of proteins and nucleic acids in solution, *Comput. Phys. Commun. 91*, 215−231.
43. Levitt, M., Hirshberg, M., Sharon, R., Laidig, K. E., and Daggett, V. (1997) Calibration and Testing of a Water Model for Simulation of the Molecular Dynamics of Proteins and Nucleic Acids in Solution, *J. Phys. Chem. B 101*, 5051−5061.
44. Zou, Q., Bennion, B. J., Daggett, V., and Murphy, K. (2002) The molecular mechanism of stabilization of proteins by TMAO and its ability to counteract the effects of urea, *J. Am. Chem. Soc. 124*, 1192−1202.
45. Leszczynski, J. F., and Rose, G. D. (1986) Loops in globular proteins: a novel category of secondary structure, *Science 234*, 849−855.
46. Clark, M. E., Burnell, E. E., Chapman, N. R., and Hinke, J. A. M. (1982) Water in barnacle muscle. IV. Factors contributing to reduced self-diffusion, *Biophys. J. 39*, 289−299.
47. Baskakov, I. V., Kumar, R., Srinivasan, G., Ji, Y. S., Bolen, D. W., and Thompson, E. B. (1999) Trimethylamine *N*-oxide-induced cooperative folding of an intrinsically unfolded transcription-activating fragment of human glucocorticoid receptor, *J. Biol. Chem. 274*, 10693−10696.
48. Baskakov, I., Wang, A. J., and Bolen, D. W. (1998) Trimethylamine-*N*-oxide counteracts urea effects on rabbit muscle lactate dehydrogenase function: a test of the counteraction hypothesis, *Biophys. J. 74*, 2666−2673.
49. Baskakov, I., and Bolen, D. W. (1998) Time-dependent effects of trimethylamine-*N*-oxide/urea on lactate dehydrogenase activity: an unexplored dimension of the adaptation paradigm, *Biophys. J. 74*, 2658−2665.
50. Peretz, D., Williamson, R. A., Matsunaga, Y., Serban, H., Pinilla, C., Bastidas, R. B., Rozenshteyn, R., James, T. L., Houghten, R. A., Cohen, F. E., Prusiner, S. B., and Burton, D. R. (1997) A conformational transition at the N terminus of the prion protein features in formation of the scrapie isoform, *J. Mol. Biol. 273*, 614−622.
51. Matsunaga, Y., Peretz, D., Williamson, A., Burton, D., Mehlhorn, I., Groth, D., Cohen, F. E., Prusiner, S. B., and Baldwin, M. A. (2001) Cryptic epitopes in N-terminally truncated prion protein are exposed in the full-length molecule: dependence of conformation on pH, *Proteins 44*, 110−118.
52. Wang, A. J., and Bolen, D. W. (1997) A naturally occurring protective system in urea-rich cells: mechanism of osmolyte

protection of proteins against urea denaturation, *Biochemistry 36*, 9101−9108.
53. Lin, T. Y., and Timasheff, S. N. (1994) Why do some organisms use a urea-methylamine mixture as osmolyte? Thermodynamic compensation of urea and trimethylamine *N*-oxide interactions with protein, *Biochemistry 33*, 12695−12701.
54. Fetrow, J. S. (1995) Omega loops: nonregular secondary structures significant in protein function and stability, *FASEB J. 9*, 708−717.
55. Ferrin, T. E., Huang, C. C., Jarvis, L. E., and Langridge, R. (1988) The MIDAS Display System, *J. Mol. Graphics 6*, 13−27.
56. Humphrey, W., Dalke, A., and Schulten, K. (1996) VMD: visual molecular dynamics, *J. Mol. Graphics 14*, 33−37.
57. Hubbard, S. J., and Thornton, J. M. (1993) *NACCESS*, Department of Biochemistry and Molecular Biology, University College, London.

BI0486379